Article

H$_2$S Sensing by Hybrids Based on Nanocrystalline SnO$_2$ Functionalized with Cu(II) Organometallic Complexes: The Role of the Ligand Platform

Marina Rumyantseva [1,*] (iD), **Ekaterina Makeeva** [1], **Alexander Gaskov** [1], **Nikolay Shepel** [2],
Svetlana Peregudova [2], **Andrey Khoroshutin** [1], **Sergey Tokarev** [1] **and Olga Fedorova** [1,2]

[1]   Faculty of Chemistry, Moscow State University, 119991 Moscow, Russia; catherine_mak@mail.ru (E.M.);
      gaskov@inorg.chem.msu.ru (A.G.); khorosh@petrol.chem.msu.ru (A.K.); pergeybokarev@gmail.com (S.T.);
      fedorova@ineos.ac.ru (O.F.)
[2]   A.N. Nesmeyanov Institute of Organoelement Compounds of Russian Academy of Sciences,
      119991 Moscow, Russia; nick7inc@ineos.ac.ru (N.S.); smp@ineos.ac.ru (S.P.)
*   Correspondence: roum@inorg.chem.msu.ru; Tel.: +7-495-939-5471

Abstract: This paper deals with the functionalization of nanocrystalline SnO$_2$ with Cu(II) complexes with organic ligands, aimed at the improvement of sensor selectivity towards gas molecules. For the synthesis of metalorganic/SnO$_2$ hybrid material complexes of Cu(II) with phthalocyanine, porphyrinines, bipyridine and azadithiacrown etherwere used. The analysis of gas sensor properties showed the possibility of increasing the sensitivity and selectivity of hybrid materials in H$_2$S detection due to the electron transfer from SnO$_2$ to an adsorbed organic molecule, which changes during the interaction between H$_2$S and Cu(II) ions.

Keywords: organic–inorganic hybrid materials; tin dioxide; Cu(II) complex; H$_2$S; semiconductor gas sensor

1. Introduction

Nanocrystalline metal oxides, mainly SnO$_2$ and ZnO, are the most common materials used to develop chemoresistive gas sensors. The mechanism of sensor signal formation [1] involves oxygen chemisorption on the oxide surface and its reaction with different reducing gases, resulting in low selectivity. Many studies have been devoted to the problem of increasing selectivity. The most promising approach is the chemical modification of the surface of semiconductor oxides, primarily clusters of metals of the platinum group, as well as oxides of transition metals that have catalytic activity in various chemical reactions [2–4].

Over the past few years, the synthesis and study of organic–inorganic hybrid nanostructures have developed significantly due to the promising possibility of creating materials with unique properties. The main advantage of using metallic complexes as a receptor part of the gas sensor is a reversible specific reaction with analytes. The correct choice of the central cation and the corresponding ligands is crucial for creating an efficient gas sensor. The central cation usually provides high selectivity in interaction with specific substances, and additional functions can be introduced by using suitable ligands. The tuning of the ligand in organic components of hybrid materials can be used as a method for modifying and optimizing the selectivity and sensitivity of the receptor function of the sensor by means of electronic and steric effects [5]. Different intermolecular forces—Lewis acid–base, dipole–dipole, hydrogen bonding, and their combination—most likely will participate in a selective interaction leading to the recognition of gas molecules.

Porphyrins and their derivative macrocycles have been studied as sensing materials in chemical sensors based on different working principles: chemoresistive, work function change, field effect, electrochemical, optical, surface plasmon resonance, mass transducing, etc. [6]. In a more straightforward approach for chemoresistive sensors, porphyrins are deposited as a solid layer directly onto conductive films. The idea is that the absorption of molecules in the porphyrin layer can change the conductivity of the underlying conductive layer [6]. For example, the influence of the Co porphyrin in the working mechanism of the SnO_2-based hybrid material is explained by the electron sensitization through the pinning of the Fermi energy due to the contact between the oxide matrix and organic component [7]. In this paper, we discuss hybrid materials based on nanocrystalline SnO_2 and Cu(II) complexes with different organic ligands. These hybrid materials can be considered as a model system in which the central ion provides selectivity in H_2S detection, and the choice of an organic ligand allows for varying the magnitude of the signal. Surface modification of *n*-type SnO_2 with *p*-type CuO is a well-known method for the selective increase of SnO_2 sensitivity to H_2S [8–23]. The selectivity mechanism for the CuO/SnO_2 system was first proposed in the earliest works of Yamazoe and co-workers [8] and confirmed for materials obtained in different forms: ceramics and thick films [11,15,22], thin films [9,12,13,16], planar thin film heterostructures [10,23], and 1D nanostructures [14,17–21]. This mechanism is associated with the formation of a system of inter-crystal *p*-CuO/*n*-SnO_2 barriers resulting in high electrical resistance in pure air. The transformation of *p*-type copper oxide into metallic copper sulfide within an interaction with H_2S leads to a significant (several orders of magnitude) decrease in the material's resistance. From the point of view of chemical bonding, it is a matter of replacing the copper–oxygen bonds with copper–sulfur bonds, combined with a reduction of copper from +2 to +1 oxidation state. Hybrid materials formed by nanocrystalline SnO_2 and metalorganic Cu(II) complexes do not contain a system of *p-n* heterojunctions and, thus, allow one to identify the interaction between Cu(II) cations and hydrogen sulfide at the molecular level, without macroscopic phase transformations, and to recognize the contribution of this process to the formation of the sensor signal.

For the synthesis of metalorganic/SnO_2 hybrid material complexes of Cu(II) with phthalocyanine (CuPc), porphyrinines (BzPh and ChPh), bipyridine (BiPy) and azadithiacrown ether (AzaCr) were used (Figure 1). Metal-phthalocyanines and metal-porphyrinines are among the most studied class of molecules for gas sensing [6], while the application of bipyridine and azadithiacrown ether Cu(II) complexes for gas sensing has not been known. At the same time, the available data indicate that macrocyclic thiaether complexes are suitable for the occurrence of electron transport reactions resulting in Cu(II)–Cu(I) transformation [24]. Also widely studied are Cu(II/I) systems containing different polypyridyl ligands: 2,2-bipyridine, 1,10-phenanthroline, and their substituted derivatives [24–26]. One example is the reduction, which was convincingly shown for the reactions of Cu(II)(diphenyldimethylbipyridine)$_2$ and Cu(II)(dimethylbipyridine)$_2$ with ferrocene and decamethylferrocene [27,28].
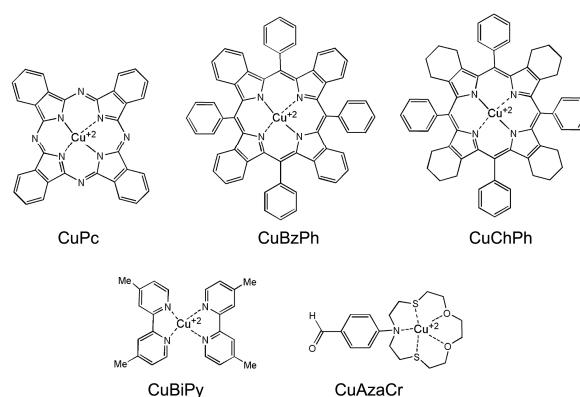

Figure 1. Structures of the metalorganic compounds used for SnO_2 modification.

2. Results and Discussion

2.1. Characteristics of Cu(II) Complexes

Copper complexes CuChPh, CuBiPy, and CuAzaCr demonstrate intensive absorption in UV and Vis regions (Figure 2a). Two peaks of absorption of CuBiPy are located at 290 and 310 nm; CuAzCr absorbs in longer wavelength region at 334 nm. The absorption spectrum of CuChPh is more complicated. It includes an intensive Q-band at 495 nm and peaks of low intensity at 290–330 nm and 550–580 nm. The combination of intensive Q-band with low intensive bands in the UV-Vis spectrum is characteristic of porphyrin derivatives [29].
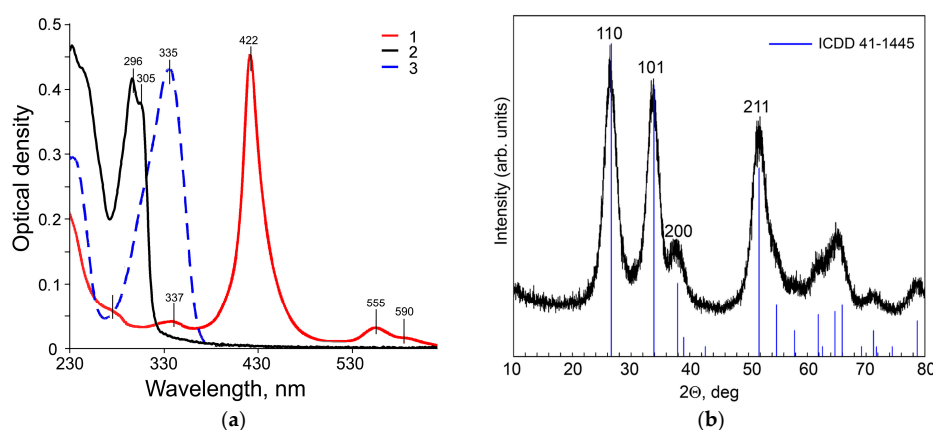
Figure 2. (**a**) UV-Vis absorption spectra of CuChPh (1); CuBiPy (2); CuAzCr (3) in CH$_3$CN; $C_{complex}$ = 3 × 10^{-5} M. (**b**) XRD pattern of nanocrystalline SnO$_2$ powder. ICDD data for SnO$_2$ cassiterite phase (41-1445) are presented as a reference.

The electrochemical properties of the compounds CuChPh, CuBiPy, and CuAzaCr were examined by cyclic voltammetry (CV). First, it was revealed that compounds CuBiPy and CuAzaCr show an irreversible oxidation at two 1.36 and 1.52 V waves (for CuBiPy) and at 1.00, 1.18, and 1.62 V waves (for CuAzaCr). The CV of compound CuChPh does not demonstrate any oxidation peaks up to the background discharge potentials. For CuBiPy and CuAzaCr complexes, irreversible reduction peaks are observed. Reduction of CuBiPy proceeds through two successive stages, the first of which is reversible, while the second is irreversible (−0.10, −1.60 V). Complex CuAzaCr showed three irreversible reduction waves (−0.96, −1.56, −2.00 V) and one reduction wave is observed for CuChPh. Onsets of the first reduction peaks (ϕ_{red}) in the CV curves for CuBiPy, CuAzaCr, and CuChPh were detected at the potentials of 0.02 V (CuBiPy), 0.90 V (CuAzaCr), and 1.06 V (CuChPh), while the onsets of the first oxidation peaks (ϕ_{ox}) are 1.30 V and 0.94 V, respectively. Based on the CV oxidation and reduction potentials, the energies of the highest occupied molecular orbitals (ϕ_{ox}/HOMO) and the lowest unoccupied molecular orbitals (ϕ_{red}/LUMO), and corresponding energy gap (E_g^{EC}) were calculated (Table 1).

Table 1. Data obtained by cyclic voltammetry, $C_{complex}$ = 10^{-3} M in CH$_3$CN, glassy carbon (GC) electrode (s = 2 mm^2), platinum plate as the counter electrode, scan rate 200 mV·s^{-1}.

| Cu(II) Complex	ϕ_{ox}/HOMO, (V)/(eV)	ϕ_{red}/LUMO, (V)/(eV)	E_g^{EC} (eV)
CuChPh	-	−1.06/−3.34	-
CuBiPy	1.30/−5.70	−0.02/−4.38	1.32
CuAzCr	0.94/−5.34	−0.90/−3.50	1.84

2.2. Characteristics of Hybrid Samples

The X-ray diffraction (XRD) pattern of nanocrystalline SnO_2 powder (Figure 2b) demonstrates the reflections of the tetragonal cassiterite phase (ICDD 41-1445) with a crystallite size of 4 nm. The specific surface area of the SnO_2 matrix is S_{surf} = 109 ± 5 m^2/g.

The control of completeness of extraction of CuBzPh, CuChPh, CuBiPy, and CuAzaCr from solutions was effectuated by a comparison of the UV-Vis absorption spectra of pure solvents, initial solutions of Cu(II) complexes, and filtrates obtained after separation of the hybrid powder samples (Figure 3). Absorption bands, which are characteristic for CuBzPh (383, 444, 510, and 644 nm) (Figure 3a), CuBiPy (295 and 310 nm) (Figure 3b), and CuAzaCr (334 nm) (Figure 3c) solutions in CH_3CN, do not appear in the absorption spectra of corresponding filtrates. This confirms that these Cu(II) complexes are completely extracted from solutions and adsorbed on the SnO_2 surface. On the other hand, in the case of CuChPh, the absorption spectra of solution in tetrahydrofuran (THF) and filtrate obtained after separation of the modified SnO_2 powder are very similar (Figure 3d). This indicates that the CuChPh concentration on the SnO_2 surface is much lower than the preassigned one. Indeed, the copper content in a CuChPh/SnO_2 hybrid sample (determined as [Cu]/[Sn] ratio by the LIMS method), 0.013 at. %, is 5–6 times lower than predicted by the synthesis conditions (0.075 at. %) (Table 2). From these data, the part of SnO_2 surface covered by Cu(II) complex (δ) was estimated as

$$\delta = \frac{d_{Å}^2 \cdot 10^{-20} \cdot N_A \cdot \alpha}{M_{SnO_2} \cdot S_{surf}} \cdot 100\%, \tag{1}$$

where N_A is Avogadro's constant, 6.022×10^{23} mol^{-1}; α = [Cu]/[Sn]; M_{SnO_2} is SnO_2 molar mass 150.7 g/mol; S_{surf} is SnO_2 specific surface area, m^2/g; and d is the maximum linear size of Cu(II) complex molecule, Å.
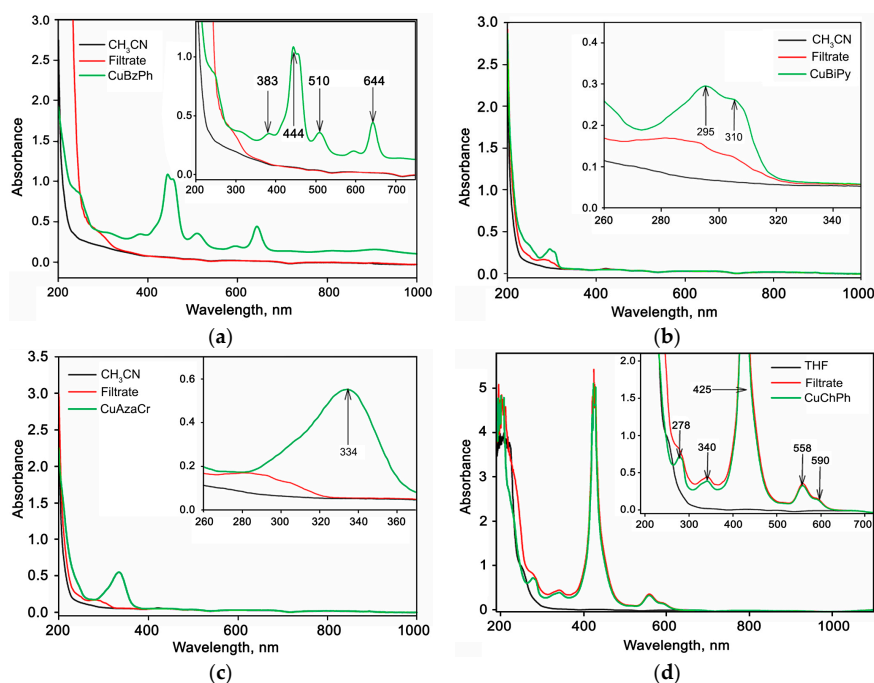
Figure 3. UV-Vis absorption spectra of pure solvents, initial solutions of Cu(II) complexes, and filtrates obtained after separation of the hybrid powder samples: (**a**) 1×10^{-4} M CuBzPh in CH_3CN; (**b**) 1×10^{-4} M CuBiPy in CH_3CN; (**c**) 1×10^{-4} M CuAzaCr in CH_3CN; (**d**) 1×10^{-4} M CuChPh in THF.

Table 2. Samples designation, composition, and resistance in pure air.

Sample	[Cu]/[Sn], at. %	Part of SnO_2 Surface Covered by Cu(II) Complex, %	Resistance at 200 °C in Pure Air R_{air}, Ohm
SnO_2	-	-	2.7×10^3
CuO/SnO_2	0.08 ± 0.02	-	2.1×10^6
$CuPc/SnO_2$	0.14 ± 0.04	11.6	6.3×10^7
$CuBzPh/SnO_2$	0.08 ± 0.02	8.9	6.5×10^7
$CuChPh/SnO_2$	0.013 ± 0.003	1.5	5.8×10^7
$CuBiPy/SnO_2$	0.07 ± 0.02	3.3	1.0×10^8
$CuAzaCr/SnO_2$	0.07 ± 0.02	4.6	8.8×10^7

Figure 4a shows the weight loss curves of SnO_2 and hybrid samples. The total weight loss of tin dioxide obtained by the sol-gel method can be due to the loss of adsorbed and bound water. The mass loss of the hybrid samples is close to the total mass loss for unmodified SnO_2, which can be explained by the low mass fraction of the organic component. However, in contrast to pure SnO_2, on the differential thermal analysis (DTA) curves (Figure 4b), for all hybrid samples there are groups of peaks characterizing exothermic processes in the temperature ranges 230–350 °C and 440–480 °C. The observed peaks probably correspond to the oxidation of organic modifiers in air, which occurs in several stages.
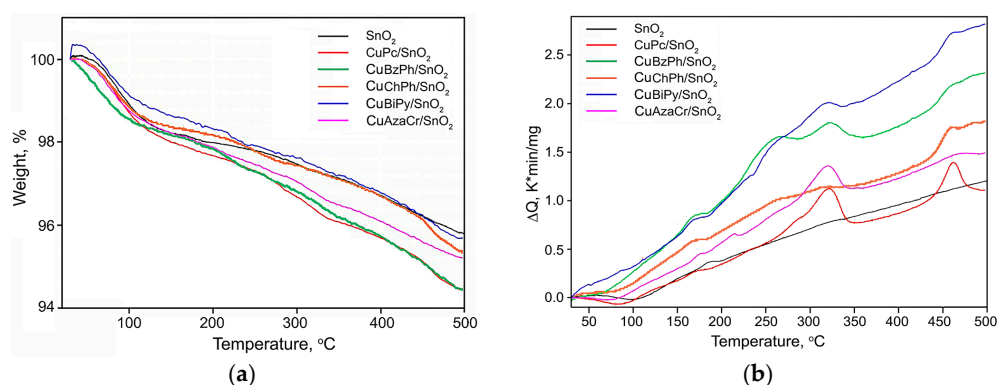

Figure 4. Weight loss (**a**) and DTA (**b**) curves of pure SnO_2 and hybrid samples.

Figure 5 reports room-temperature Raman spectra of the hybrid powder samples. Two Raman active modes of SnO_2 are observed: A_{1g} (630 cm^{-1}) and B_{2g} (772 cm^{-1}) (Figure 5a). The spectra also exhibit a broad feature around the A_{1g} mode, attributed to surface modes [30]. For comparison, all spectra were normalized to the intensity of the A_{1g} mode.

Raman spectra of $CuPc/SnO_2$ and $CuBiPy/SnO_2$ samples in the 750–1900 cm^{-1} range (Figure 5b) correlate well with the spectra of individual complexes CuPc and $[Fe(bpy)_3]^{2+}$ [31,32]. In the case of the complex CuBiPy, containing dimetilbipyridin instead of bipyridine in $[Fe(bpy)_3]^{2+}$, in the Raman spectrum of the synthesized hybrid sample there are additional bands corresponding to the vibrations of –CH$_3$ groups (1380 and 1460 cm^{-1}). The Raman bands in the spectrum of $CuAzaCr/SnO_2$ sample in this range correspond to the main structural elements of the modifier molecule [31–33].

The spectrum of $CuBzPh/SnO_2$ sample in the range of 750–1900 cm^{-1} also indicates the presence of the organic complex on SnO_2 surface because it contains the characteristic bands of the main structural elements of modifier molecule (aromatic carbon- and nitrogen-containing rings), including a mode at 1610 cm^{-1} corresponding to the vibrations of double C=C and C=N bonds. At the same time, the Raman spectrum of the hybrid sample $CuChPh/SnO_2$ containing a ChPh modifier structurally close to BzPh does not contain the corresponding characteristic modes. This may be caused by a low concentration of this organic complex on the SnO_2 surface (Table 2).

For all hybrid samples in the range 2700–3200 cm^{-1}, the Raman spectra recorded at room temperature have characteristic modes corresponding to the C–H vibrations in the aliphatic groups (Figure 5a). However, only three of the five Cu(II) organic complexes used in this work contain –CH$_3$ and –CH$_2$- -groups in their structure: CuChPh/SnO$_2$ (–CH$_2$- -group of cyclohexene ring), CuBiPy/SnO$_2$ (–CH$_3$ groups of dimethylpyridine), and CuAzaCr/SnO$_2$ (–CH$_2$- -group of crown ether ring). In the case of CuPc/SnO$_2$ and CuBzPh/SnO$_2$ samples, the appearance of these bands may be caused by the presence of CH$_3$CN adsorbed on the surface of tin dioxide during modification with Cu(II) organic complexes by adsorption from solution.
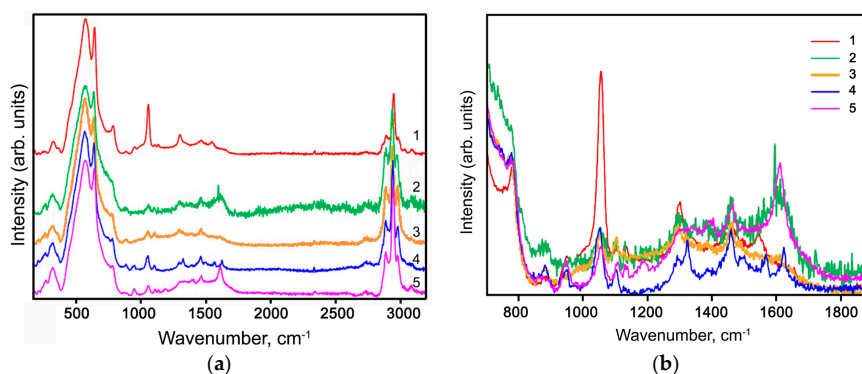
Figure 5. Room-temperature Raman spectra of hybrid powder samples (1) CuPc/SnO$_2$, (2) CuBzPh/SnO$_2$, (3) CuChPh/SnO$_2$, (4) CuBiPy/SnO$_2$, (5) CuAzaCr/SnO$_2$ in the spectral range of (**a**) 172–3200 cm^{-1}; (**b**) 700–1900 cm^{-1}.

Raman spectra of hybrid CuPc/SnO$_2$ sample recorded under in situ step heating up to 500 °C are shown in Figure 6a. The analogous spectra of the CuPc/SnO$_2$, CuChPh/SnO$_2$, CuBiPy/SnO$_2$, and CuAzaCr/SnO$_2$ samples, recorded at 300 °C, and spectrum of CuBzPh/SnO$_2$, recorded at 250 °C (Figure 6b), do not contain bands corresponding to the vibrations of organic structures, reflecting their complete thermal decomposition. At the same time, the spectra recorded at 200 °C for all hybrid samples still contain the characteristic bands of organic compounds. These results agree with the data obtained from thermal analysis. In this regard, in subsequent studies of gas sensor properties of hybrid materials the measurement temperature did not exceed 200 °C.
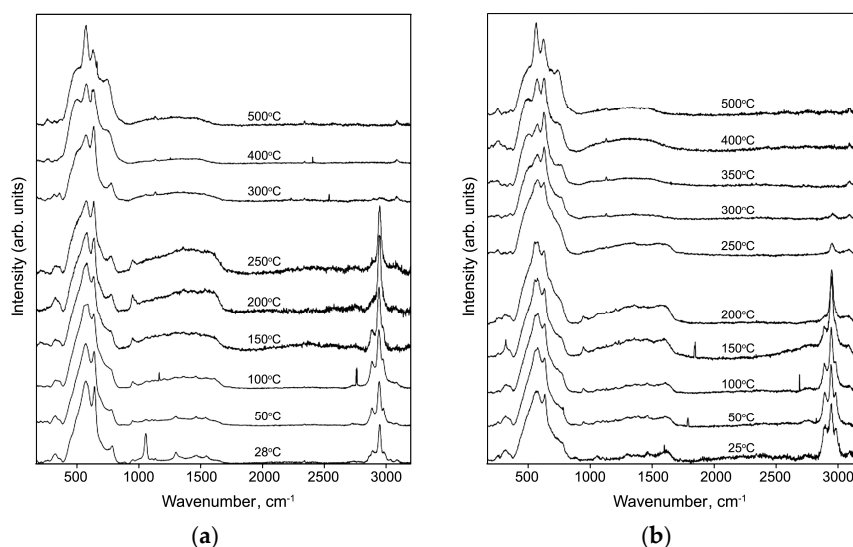
Figure 6. Raman spectra of CuPc/SnO$_2$ (**a**) and CuBzPh/SnO$_2$ (**b**) hybrid samples recorded under in situ step heating up to 500 °C.

2.3. Electrophysical and Gas Sensor Properties

Modification of tin dioxide surface with Cu(II) organic complexes results in a significant growth of resistivity of hybrid samples as compared with blank SnO_2 and even with CuO/SnO_2 reference sample (Table 2). A model for energy level alignment of the first organic molecular layer on the oxide substrate was proposed in [34]. Since the molecules of organic complexes are in direct contact with the semiconductor oxide, their electronic systems are interconnected. If the work function of the oxide φ is greater than the ionization potential of the organic molecule I_E, $\varphi > I_E$, the positively charged state of organic molecules is thermodynamically favorable. In this case, electrons will be transferred from the organic semiconductor to the oxide substrate. However, if $\varphi < I_E$, there is no electron transfer from organic layer to the oxide. The situation $\varphi < I_E$ is realized in the case of $CuPc/SnO_2$, $CuBiPy/SnO_2$, and $CuAzaCr/SnO_2$ hybrid samples ($I_E(CuPc) = 5.41 \div 6.48$ eV [35], I_E (CuBiPy) = 5.70 eV, I_E (CuAzaCr) = 5.34 eV, φ (SnO_2) = 4.7 eV [36]) (Figure 7). Since the HOMO orbital (b_{1g}) of Cu(II) complexes is half-filled [37], and is lower in energy than the Fermi level of SnO_2, electron transfer from the oxide surface to the adsorbed organic molecule becomes possible. This results in the decrease of free carrier concentration in the near surface layer of the *n*-type semiconductor in comparison with the crystal bulk. The bulk charge formed owing to the interaction in the near surface layer induces band bending, and a growth in barrier height at SnO_2 grain boundaries. These two factors are responsible for the resistivity increase of hybrid samples $CuPc/SnO_2$, $CuBiPy/SnO_2$, and $CuAzaCr/SnO_2$. An analogous increase in the resistance of hybrid materials with other Cu(II) complexes allows us to assume a similar electronic structure of the interface between the organic molecules and SnO_2.
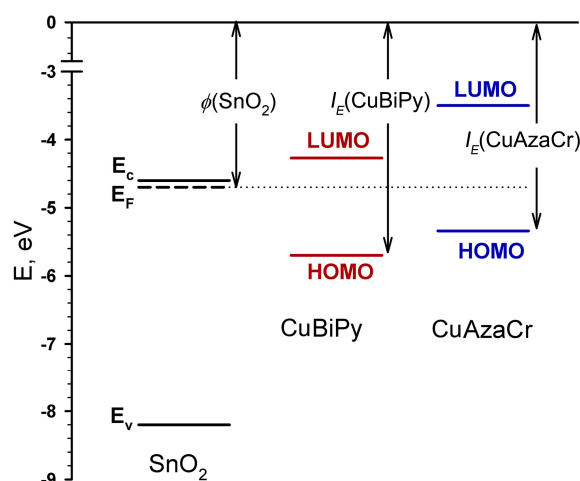
Figure 7. A diagram reflecting the relative positions of the energy levels for bulk SnO_2 and CuBiPy and CuAzaCr complexes: conduction band E_c, valence band E_v, Fermi level E_F, work function φ, ionization energy I_E.

Figure 8a shows the dynamic electrical response of blank SnO_2, reference sample CuO/SnO_2 and hybrid samples to the periodical change of gas phase composition from dry air to 1 ppm $H_2S/$air at 200 °C. A stable, reproducible sensor signal was obtained for all the samples in the presence of each of the target gases (CO, NH_3, H_2S). Since the resistance of hybrid samples decreases in the presence of reducing gases, their behavior corresponds to *n*-type semiconductors.
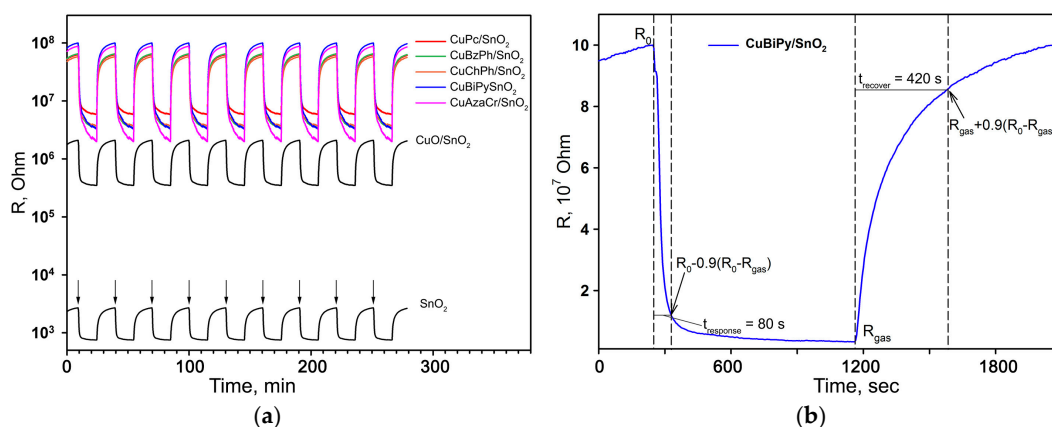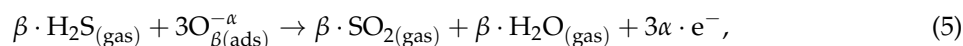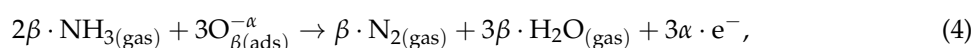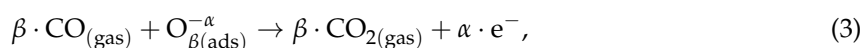
Figure 8. (**a**) The electrical response of different samples to the periodical change of gas phase composition from dry air to 1 ppm H_2S/air at 200 °C; (**b**) The electrical response (1 cycle) and dynamic characteristics of CuBiPy/SnO_2 hybrid sample.

The nature of the sensor signal in semiconductors is associated predominantly with chemisorption involving free electrons in the subsurface layer of the material. The equation describing the oxygen chemisorption can be written as [1]:

$$\frac{\beta}{2}O_{2(gas)} + \alpha \cdot e^- \rightarrow O^{-\alpha}_{\beta(ads)},\tag{2}$$

where $O_{2(gas)}$ is an oxygen molecule in the ambient atmosphere, $O^{-\alpha}_{\beta(ads)}$ is an atomic or molecular form of chemisorbed oxygen on SnO_2 surface, e is an electron, which can reach the surface. A decrease in the electrical resistance in the presence of reducing gas CO, NH_3, or H_2S could be explained by the following redox reactions:

$$\beta \cdot CO_{(gas)} + O^{-\alpha}_{\beta(ads)} \rightarrow \beta \cdot CO_{2(gas)} + \alpha \cdot e^-,\tag{3}$$

$$2\beta \cdot NH_{3(gas)} + 3O^{-\alpha}_{\beta(ads)} \rightarrow \beta \cdot N_{2(gas)} + 3\beta \cdot H_2O_{(gas)} + 3\alpha \cdot e^-,\tag{4}$$

$$\beta \cdot H_2S_{(gas)} + 3O^{-\alpha}_{\beta(ads)} \rightarrow \beta \cdot SO_{2(gas)} + \beta \cdot H_2O_{(gas)} + 3\alpha \cdot e^-,\tag{5}$$

where e is an electron injected into the conduction band of the semiconductor oxide.

The response time $t_{response}$ (the time required to reach 90% of the maximum sensor signal) and the recovery time $t_{recovery}$ (the time required for 90% of the sensor response change after removal of the target gas CO, NH_3, or H_2S from the gas phase) were determined from the dynamic response curves, as is shown in Figure 8b. At the measurement temperature of 200 °C, for all the samples and all gases under discussion the $t_{response}$ and $t_{recovery}$ values are 70–80 s and 400–420 s, respectively. Taking into account that these values are close for blank SnO_2 and hybrid samples, it can be assumed that $t_{response}$ and $t_{recovery}$ are determined by the thickness of the sensitive layer and the characteristics of its porous structure formed during sintering.

Figure 9 compares the sensor signal to CO (40 ppm), NH_3 (450 ppm), and H_2S (1 ppm) for bare SnO_2, reference CuO/SnO_2, and hybrid samples. The values of sensor signal toward CO and NH_3 depend weakly on the composition of the sensitive material. It is known [38] that for SnO_2-based materials the sensor signal toward CO (reducing gas without pronounced acid/base properties) at 200 °C correlates with the specific surface area of semiconductor oxide, type of predominant form of chemisorbed oxygen and its concentration. Since modification of SnO_2 surface with Cu(II) organic complexes does not influence these parameters, it also has no effect on SnO_2 reactivity in interaction with CO. When detecting NH_3 (Lewis base) in dry air, the sensor signal correlates with the
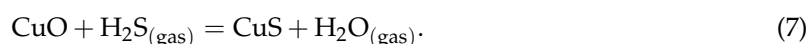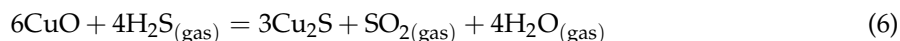
surface concentration of corresponding acid sites [39,40]. As Cu(II) is a weaker acid than Sn(IV) [41], its presence on the SnO$_2$ surface does not increase the sensitivity of the hybrid materials towards ammonia.
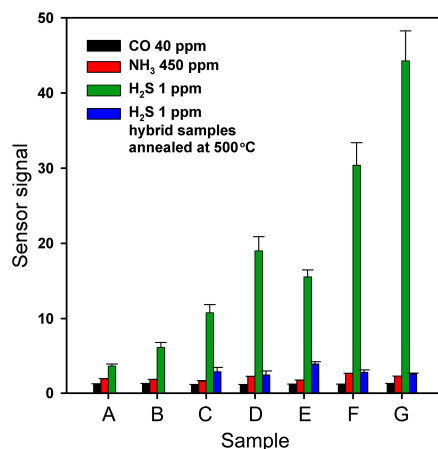
Figure 9. Sensor signal to CO (40 ppm), NH$_3$ (450 ppm), and H$_2$S (1 ppm) for different samples: (A) SnO$_2$; (B) CuO/SnO$_2$; (C) CuPc/SnO$_2$; (D) CuBzPh/SnO$_2$; (E) CuChPh/SnO$_2$; (F) CuBiPy/SnO$_2$; (G) CuAzaCr/SnO$_2$.

Hydrogen sulfide is a Brønsted acid, and heterolytic breaking of the S–H bond is quite easy, especially in the formation of new donor–acceptor bonds [42]. In CuO/SnO$_2$ nanocomposites, the significant resistance change in the presence of H$_2$S is attributed to the formation of Cu$_2$S (narrow-gap semiconductor, band gap 1.2 eV) or CuS (metallic conductor) [11]:

$$6CuO + 4H_2S_{(gas)} = 3Cu_2S + SO_{2(gas)} + 4H_2O_{(gas)} \tag{6}$$

$$CuO + H_2S_{(gas)} = CuS + H_2O_{(gas)}. \tag{7}$$

These reactions result in the removal of the *n*-SnO$_2$/*p*-CuO heterocontacts, which leads to a decrease in inter-crystal barriers in the sensitive layer, accompanied by a significant decrease in the sensor's resistance [8]. In the case of the reference sample (CuO/SnO$_2$) used in the present work, this mechanism is not fully manifested, possibly because of the copper concentration in the sample being too low to provide the necessary quantity of the *n*-SnO$_2$/*p*-CuO heterocontacts. However, in the case of H$_2$S detection the hybrid samples demonstrate a significantly increased sensor signal. With the additional annealing of all the hybrid samples at 500 °C resulting in the formation of oxide composite samples, the values of the sensor signal to 1 ppm of H$_2$S in the air become comparable with those of the CuO/SnO$_2$ reference sample. This indicates that in hybrid samples an additional sensing mechanism is realized, in which Cu(II) organic complexes are involved.

One can suppose that in the presence of H$_2$S the electronic interaction between the HOMO (b_{1g}) orbital of Cu(II) complex and the electronic system of SnO$_2$ surface is influenced by a strong interaction between the Cu b_{1g} orbital and the π^* orbital of S^{2-}. This may be interpreted in the frame of the *trans effect* concept, which postulates that the two ligands in a trans position compete for the same metal d-orbitals. In other words, there is a competition between the two axial coordination bonds, the "Cu–surface" and the "Cu–S^{2-}" bonds [43]. This trans influence is attributed to S^{2-}, which is considered a ligand that has a strong trans effect [44]. This interaction leads to a stronger energy separation between the bonding and antibonding orbitals, as a result of which the latter can now be above the Fermi level of SnO$_2$. Therefore, the S^{2-} ligand weakens the interaction between Cu(II) and SnO$_2$ substrate and the electron transfer from SnO$_2$ surface to the Cu(II) ion is suppressed [43]. This results, in turn, in a decrease of resistivity in hybrid samples forming the sensor signal to H$_2$S.

Obviously, that the composition and design of the ligand platform play a critical role in controlling the activities and structures of the copper complexes. The complexes investigated in this research can be divided into two groups. The first includes the porphyrin and phthalocyanine Cu(II) complexes and the second includes the bipyridine and azathiacrown ether complexes. The first type of complex forms when the hydrogen ions of N–H of the porphyrin or phthalocyanine were replaced by metal ions. In the porphyrin and phthalocyanine Cu(II) complexes the central metal ion is bound with a ligand through the strong four hybrid covalent–coordination bonds with N-heteroatoms of pyrrole rings. This makes very stable metalorganic compounds. In the second type the Cu(II) ion is bound with bipyridine heterocycles or azathiacrown ether through coordination bonds, which are not very stable. This coordination is not very strong. It means that when an additional ligand such as a gas molecule appears, the complex can be easily reorganized to interact with the novel ligand.

In addition, copper–thiaether complexes demonstrate a charge transfer of S-Cu(II), as a result of which Cu(II) in thiaether complexes is easily reduced to Cu(I) in a reversible manner [45,46]. Thus, the electron transfer between metal and ligand in copper–thiaether complexes simulates the redox reaction. The ligand–metal charge transfer process is also known to take place in the bipyridine complex of Cu(II) [47]. Redox-driven Cu(II)/Cu(I) transfer was found in the composition of the bipyridine complex [48]. This reduction of copper further contributes to the change of resistivity of CuBiPy/SnO$_2$ and CuAzaCr/SnO$_2$ hybrid samples. Based on X-ray photoelectron spectroscopy (XPS) studies [49] and X$_\alpha$-calculations [50], it can be expected that the added electron will occupy the b_{1g} orbital resulting in the d^{10} configuration [37]. This will lead to a situation where the HOMO orbital of the Cu(II) complex is completely filled and electron transfer from oxide to the complex becomes impossible. This will result in a more significant decrease of resistivity of CuBiPy/SnO$_2$ and CuAzaCr/SnO$_2$ hybrid samples, providing greater sensor signal.

Table 3 presents a comparative analysis of some characteristics of H$_2$S sensors based on *p*-CuO/*n*-SnO$_2$ semiconductor materials. In all cases, the same mechanism of sensor signal, based on the formation and removal of the energy barrier between *p*-CuO and *n*-SnO$_2$, is realized; however, the values of the sensor signal vary greatly depending on the parameters of the nanostructure of the materials and the [Cu]/[Sn] ratio.

Table 3. H$_2$S sensors based on *p*-CuO/*n*-SnO$_2$ semiconductor materials.

Type of Sensitive Material	H$_2$S Concentration, ppm	Operating Temperature, °C	Sensor Signal	Reference
Ceramic	50	200	3.5×10^4	[8]
Ceramic	300	100	5.0×10^2	[11]
Thick film	1	50	8.0×10^3	[15]
Thin film	100	150	1.0×10^4	[9]
Thin film	100	200	1.0×10^2	[12]
Thin film	50	200	2.5×10^4	[13]
Thin film	68.5	RT	3.6×10^3	[16]
Planar heterostructure	100	160	1.7×10^4	[10]
Nanoribbons	3	RT	1.7×10^2	[14]
Nanowires	16	150	2.0×10^6	[17]
Nanowires	20	300	8.0×10^2	[18]
Nanowires	1	300	2	[19]
Nanowires	1	200	7.0×10^2	[20]
Nanowire (individual)	10	200	2.6×10^1	[21]
Hybrid material CuAzaCr/SnO$_2$	1	200	4.3×10^1	This work

For the H$_2$S concentration of 1 ppm, the sensor signal of different materials varies from *S* = 2 [19] to *S* = 8000 [15]. The hybrid materials obtained in this work are sensitive enough (*S* = 43 in the case of CuAzaCr/SnO$_2$) to allow detection of practically important low concentrations of hydrogen sulfide (recommended threshold limit values are 1 ppm for an eight-hour time weighted average (TWA) and

5 ppm for short-term exposure limit (STEL)). Obviously, further improvement of the sensor signal can be achieved by the optimization of the ligand platform and [Cu]/[Sn] ratio. The development of organic–inorganic hybrid materials can be an effective way to fine tune the sensitivity and selectivity of materials for gas sensors.

3. Materials and Methods

3.1. Materials Synthesis

3.1.1. Synthesis of Cu(II) Complexes

Cu(II)-phthalocyanine (CuPc) was supplied by Merck(Darmstadt, Germany) and used without further purification. Porphyrins BzPh and ChPh were prepared according to [29]. Cu(II) porphyrins CuBzPh and CuChPh have been synthesized as in [29] from 0.1 mmol of metal-free ligands BzPh or ChPh with 0.2 mmol Cu(OAc)$_2$ in 30 mL of refluxing DMF for 6 h. The Cu(II) complex CuBzPh has been obtained with 70% yield; Cu(II) complex CuChPh has been isolated with 62% yield.

The bipyridine BiPy is commercially available from Merck (Darmstadt, Germany); azadithiacrown ether AzaCr was obtained according to [51,52]. The bipyridine CuBiPy and azadithiacrown ether CuAzaCr complexes with Cu(II) were obtained according to the known procedures described in [53,54] and [51,52], respectively.

3.1.2. Synthesis of Nanocrystalline SnO$_2$ and Hybrid Materials

Nanocrystalline tin dioxide (SnO$_2$) was obtained by hydrolysis of tin (IV) chloride using commercial 25% aqueous ammonia (NH$_3\cdot$H$_2$O), with subsequent thermal annealing at 300 °C for 24 h [38]. For modification, 0.1 g of SnO$_2$ was immersed into 5 mL of 1×10^{-4} M solution of Cu(II) complex (Figure 1). The solvents used were acetonitrile (CH$_3$CN) for CuBzPh, CuBiPy, and CuAzaCr, and tetrahydrofuran (THF) for CuChPh. The obtained suspensions were stirred at room temperature for 2 h. Then hybrid powders were precipitated by centrifugation, washed several times with small portions of the solvent, and dried at 35 °C for 3 h.

Since CuPc has extremely low solubility in common solvents [55] to effectuate the modification, 39.2 mg CuPc and 1.25 g SnO$_2$ were stirred in 25 mL CH$_3$CN at room temperature for 4 h. Then the hybrid powder was precipitated by centrifugation, washed several times with small portions of CH$_3$CN, and dried at 35 °C for 3 h.

Reference sample CuO/SnO$_2$—CuO modified SnO$_2$ ([Cu]/[Sn] = 0.075 at. %)—was obtained via impregnation of SnO$_2$ dried gel with 0.03 M aqueous solution of Cu(CH$_3$COO)$_2$ with subsequent annealing at 300 °C for 24 h.

3.2. Materials Characterization

The absorption spectra of organic Cu(II) complexes in UV-Vis regions (200–800 nm wavelength range) were recorded using a Varian Cary 50 spectrometer (Varian Inc., Palo Alto, CA, USA).

Cyclic voltammetry measurements were performed on a IPC-Pro M potentiostat for ca. 10^{-3} M solutions of CuChPh, CuBiPy, and CuAzaCr complexes in rigorously dried acetonitrile in a standard three-electrode cell equipped with a glassy carbon (GC) working electrode ($s = 2$ mm^2), Pt plate as the counter electrode, and saturated calomel electrode (SCE) as a reference electrode. The scan rate was 200 mV$\cdot$s^{-1}. A solution containing 0.1 M Bu$_4$NPF$_6$ was used as the supporting electrolyte.

The energies of HOMO and LUMO of the compounds CuBiPy and CuAzaCr were obtained from the first oxidation and reduction potential, respectively. Compounds CuBiPy and CuAzaCr demonstrated irreversible oxidation and reduction processes. This is why the potentials when the intensity of corresponding CV curve increases (ϕ_{red} and ϕ_{ox} in Equations (8) and (9)) were used as oxidation and reduction potentials. The energy level of the normal hydrogen electrode (NHE) is

situated at 4.40 eV, below the zero vacuum energy level [56,57]. A simple relation can be written that allows for the estimation of both energy values (Equations (8) and (9)):

$$LUMO = -e(\phi_{red} + 4.40) \ (eV) \tag{8}$$

$$HOMO = -e(\phi_{ox} + 4.40) \ (eV). \tag{9}$$

Phase composition was determined by X-ray powder diffraction (XRD) using the Rigaku diffractometer (λ =1.54059 Å ($CuK_{\alpha 1}$ radiation)). The crystallite size (d_{XRD}) of SnO_2 was estimated from the broadening of 110 and 101 XRD peaks using the Scherrer equation.

The specific surface area of SnO_2 powder was determined by low-temperature nitrogen adsorption; the calculations were performed using the Brunauer–Emmett–Teller (BET) method. The measurements were performed in a single-point mode on a Chemisorb 2750 instrument (Micromeritics, Norcross, GA, USA) at 77 K using a N_2:He gas mixture containing 30 vol. % N_2.

The control of complete adsorption of organic Cu(II) complexes from solution was effectuated by UV-Vis optical spectroscopy using a Varian Cary 50 spectrometer (Varian Inc., Palo Alto, CA, USA). The absorbance spectra of initial solutions, filtrates after adsorption, and pure solvents were recorded in the wavelength range of 1100–200 nm.

The analysis of Cu concentration in hybrid samples (as [Cu]/[Sn] ratio in at. %) was effectuated by laser-induced mass spectrometry using the EMAL-2 setup (Concern-Electron, Lviv, Ukraine). Thermogravimetric analysis (TGA) was performed using the NETZSCH STA 409 PC/PG (Netzsch-Gerätebau GmbH, Selb, Germany) technique. The samples were heated in air from room temperature up to 500 °C with a heating rate of 10 °C/min.

Raman spectra were collected using a Renishaw spectrometer (Renishaw plc, New Mills, UK). The green line of an Ar laser (514.53 nm) in micro-Raman configuration (objective 50×) was used. The laser power did not exceed 10 mW in order to prevent the strong heating of the sample. The spectra were recorded in air at room temperature and in situ under heating from room temperature to 500 °C in increments of 50–100 °C.

For the gas sensing experiments, the materials were mixed with a vehicle (α-terpineol in ethanol) and deposited as thick films (~1 μm thick) by the drop-coating technique over functional alumina substrates (~120 μm thick), having Pt contacts on the front side and a Pt-heater on the back. The thick films were dried at 30 °C for 24 h and sintered at 200 °C for 24 h in air. The deposition method allows us to obtain continuous and uniform coatings. The films have a porous structure formed of agglomerated particles [58]. All sensor measurements were carried out in a flow cell with a controlled constant flow of 200 mL/min. Certified gas mixtures were used as sources of target gases. The composition of the atmosphere was determined by electronic mass flow controllers (Bronkhorst, Ruurlo, Netherlands). Direct current (DC) measurements (U = 3 V) have been carried out in the presence of CO (40 ppm), NH_3 (450 ppm), and H_2S (1 ppm) in dry air. The sensor signal S was calculated as $S = R_{air}/R_{gas}$, where R_{gas} is the resistance of the sample in the presence of reducing gas (CO, NH_3, H_2S) and R_{air} is the resistance in pure air.

4. Conclusions

Hybrid organic–inorganic gas-sensitive materials with high sensitivity and selectivity in H_2S detection were obtained through functionalization of nanocrystalline SnO_2 with Cu(II) complexes with different organic ligands. This modification results in a significant growth of resistivity of hybrid samples as compared with blank SnO_2 and even with CuO/SnO_2 reference sample. This fact is explained by the decrease in the concentration of free carriers in the near-surface layer of an *n*-type semiconductor because of the electron transfer from the oxide surface to the adsorbed organic molecule. In the presence of H_2S, the electronic interaction between the HOMO (b_{1g}) orbital of the Cu(II) complex and the electronic system of the SnO_2 surface is influenced by the strong interaction between the Cu b_{1g} orbital and the π^* orbital of S^{2-}, which suppresses the transfer of electrons from the semiconductor

to the Cu(II) ion. It was observed that the composition and design of the ligand platform play a critical role in controlling the activities and structures of the copper complexes. The reduction of copper additionally contributes to the change of resistivity of hybrid samples, where Cu(II) ion is bound with bipyridine heterocycles or azathiacrown ether through the coordination bonds, providing a higher sensor signal.

Author Contributions: Ekaterina Makeeva synthesized the hybrid samples and performed the experiments. Marina Rumyantseva designed the experiments and wrote the manuscript. Alexander Gaskov formulated the concept of this work and participated in the discussion of the results. Sergey Tokarev, Andrey Khoroshutin, and Nikolay Shepel synthesized and characterized organic complexes. Svetlana Peregudova effectuated electrochemical experiments. Olga Fedorova contributed to the synthesis and characterization of organic complexes and in the writing of the manuscript.

Conflicts of Interest: The authors declare no conflict of interest.

References

1. Bârsan, N.; Weimar, U. Conduction Model of Metal Oxide Gas Sensors. *J. Electroceram.* **2001**, *7*, 143–167. [CrossRef]
2. Korotcenkov, G. *Handbook of Gas Sensor Materials. Properties, Advantages and Shortcomings for Applications*; Springer: New York, NY, USA, 1997; Volume 1, pp. 273–286.
3. Krivetskiy, V.V.; Rumyantseva, M.N.; Gaskov, A.M. Chemical modification of nanocrystalline tin dioxide for selective gas sensors. *Russ. Chem. Rev.* **2013**, *82*, 917–941. [CrossRef]
4. Korotcenkov, G.; Cho, B.K. Metal oxide composites in conductometric gas sensors: Achievements and challenges. *Sens. Actuators B-Chem.* **2017**, *244*, 182–210. [CrossRef]
5. Korotcenkov, G. *Handbook of Gas Sensor Materials. Properties, Advantages and Shortcomings for Applications*; Springer: New York, NY, USA, 1997; Volume 2, pp. 155–164.
6. Paolesse, R.; Nardis, S.; Monti, D.; Stefanelli, M.; Di Natale, C. Porphyrinoids for Chemical Sensor Applications. *Chem. Rev.* **2017**, *117*, 2517–2583. [CrossRef] [PubMed]
7. Callone, E.; Carturan, G.; Ischia, M.; Epifani, M.; Forleo, A.; Siciliano, P.; Paolesse, R. The hydrolytic route to Co-porphyrin-doped SnO_2 gas-sensing materials: Chemical study of Co-porphyrin versus Sn(IV) oxide interactions. *Inorg. Chim. Acta* **2008**, *361*, 79–85. [CrossRef]
8. Tamaki, J.; Maekawa, T.; Miura, N.; Yamazoe, N. CuO-SnO_2 element of highly sensitive and selective detection of H_2S. *Sens. Actuators B-Chem.* **1992**, *9*, 197–203. [CrossRef]
9. Rumyantseva, M.N.; Labeau, M.; Delabouglise, G.; Ryabova, L.I.; Kutsenok, I.B.; Gaskov, A.M. Copper and nickel doping effect on interaction of SnO_2 films with H_2S. *J. Mater. Chem.* **1997**, *7*, 1785–1790. [CrossRef]
10. Vasiliev, R.B.; Rumyantseva, M.N.; Yakovlev, N.V.; Gaskov, A.M. CuO/SnO_2 thin film heterostructures as chemical sensors to H_2S. *Sens. Actuators B-Chem.* **1998**, *50*, 187–194. [CrossRef]
11. Boulova, M.; Galerie, A.; Gaskov, A.; Lucazeau, G. Reactivity of SnO_2-CuO nanocrystalline materials with H_2S: A coupled electrical and Raman spectroscopic study. *Sens. Actuators B-Chem.* **2000**, *71*, 134–139.
12. Nirajan, R.S.; Patil, K.R.; Sainkar, S.R.; Mulla, I.S. High H_2S-sensitive copper-doped tin oxide thin film. *Mater. Chem. Phys.* **2003**, *80*, 250–256. [CrossRef]
13. Katti, V.R.; Debnath, A.K.; Muthe, K.P.; Kaur, M.; Dua, A.K.; Gadkari, S.C.; Gupta, S.K.; Sahni, V.C. Mechanism of drifts in H_2S sensing properties of SnO_2:CuO composite thin film sensors prepared by thermal evaporation. *Sens. Actuators B-Chem.* **2003**, *96*, 245–252. [CrossRef]
14. Kong, X.; Li, Y. High sensitivity of CuO modified SnO_2 nanoribbons to H_2S at room temperature. *Sens. Actuators B-Chem.* **2005**, *105*, 449–453. [CrossRef]
15. Patil, L.A.; Patil, D.R. Heterocontact type CuO-modified SnO_2 sensor for the detection of a ppm level H_2S gas at room temperature. *Sens. Actuators B-Chem.* **2006**, *120*, 316–323. [CrossRef]
16. Gong, S.P.; Xia, J.; Liu, J.Q.; Zhou, D.X. Highly sensitive SnO_2 thin film with low operating temperature prepared by sol–gel technique. *Sens. Actuators B-Chem.* **2008**, *134*, 57–61.
17. Kumar, V.; Sen, S.; Muthe, K.P.; Gaur, N.K.; Gupta, S.K.; Yakhmi, J.V. Copper doped SnO_2 nanowires as highly sensitive H_2S gas sensor. *Sens. Actuators B-Chem.* **2009**, *138*, 587–590. [CrossRef]

18. Hwang, I.S.; Choi, J.K.; Kim, S.-J.; Dong, K.Y.; Kwon, J.H.; Ju, B.K.; Lee, J.H. Enhanced H$_2$S sensing characteristics of SnO$_2$ nanowires functionalized with CuO. *Sens. Actuators B-Chem.* **2009**, *142*, 105–110. [CrossRef]

19. Kim, S.S.; Na, H.G.; Choi, S.-W.; Kwak, D.S.; Kim, H.W. Novel growth of CuO-functionalized, branched SnO$_2$ nanowire and their application to H$_2$S sensors. *J. Phys. D. Appl. Phys.* **2012**, *45*, 205301-1–205301-8. [CrossRef]

20. Mathur, S.; Giebelhaus, I.; Fischer, T.; Morante, J.R.; Arbiol, J.; Gaskov, A.; Rumyantseva, M.; Varechkina, E.; Ivanov, V. One-dimensional CuO-SnO$_2$ *p-n* heterojunctions for enhanced detection of H$_2$S. *J. Mater. Chem. A* **2013**, *1*, 11261–11268.

21. Shao, F.; Hoffmann, M.W.G.; Prades, J.D.; Zamani, R.; Arbiol, J.; Morante, J.R.; Varechkina, E.; Rumyantseva, M.; Gaskov, A.; Giebelhaus, I.; et al. Heterostructured *p*-CuO (nanoparticle)/*n*-SnO$_2$ (nanowire) devices for selective H$_2$S detection. *Sens. Actuators B-Chem.* **2013**, *181*, 130–135. [CrossRef]

22. Guo, Z.; Chen, G.; Zeng, G.; Liu, L.; Zhang, C. Metal oxides and metal salt nanostructures for hydrogen sulfide sensing: Mechanism and sensing performance. *RSC Adv.* **2015**, *5*, 54793–54805. [CrossRef]

23. Boroun, Z.; Ghorbani, M.; Moosavi, A.; Mohammadpour, R. New Insight into H$_2$S Sensing Mechanism of Continuous SnO$_2$−CuO Bilayer Thin Film: A Theoretical Macroscopic Approach. *J. Phys. Chem. C* **2016**, *120*, 7678–7684. [CrossRef]

24. Rorabacher, D.B. Electron Transfer by Copper Centers. *Chem. Rev.* **2004**, *104*, 651–697. [CrossRef] [PubMed]

25. Doine, H.; Yano, Y.; Swaddle, T.W. Kinetics of the bis(2,9-dimethyl-1,10-phenanthroline)copper(I/II) self exchange reaction in solution. *Inorg. Chem.* **1989**, *28*, 2319–2322. [CrossRef]

26. Clemmer, J.D.; Hogaboom, G.K.; Holwerda, R.A. Reduction of the bis(2,9-dimethyl-1,10-phenanthroline)copper(II) ion by substituted hydroquinones. *Inorg. Chem.* **1979**, *18*, 2567–2572. [CrossRef]

27. Koshino, N.; Kuchiyama, Y.; Funahashi, S.; Takagi, H.D. Electron self-exchange, oxidation, and reduction reactions of bis(2,9-dimethyl-4,7-diphenyl-1,10-phenanthroline)copper(II/I) and bis(6,6′-dimethyl-2,2′-bipyridine)copper(II/I) couples in acetonitrile: Gated ET for the reduction, oxidation, and self-exchange processes. *Can. J. Chem.* **1999**, *77*, 1498–1507.

28. Koshino, N.; Kuchiyama, Y.; Ozaki, H.; Funahashi, S.; Takagi, H.D. An Interpretation of Gated Behavior: Kinetic Studies of the Oxidation and Reduction Reactions of Bis(2,9-dimethyl-1,10-phenanthroline)copper(I/II) in Acetonitrile. *Inorg. Chem.* **1999**, *38*, 3352–3360. [CrossRef] [PubMed]

29. Sato, T.; Mori, W.; Kato, C.N.; Yanaoka, E.; Kuribayashi, T.; Ohtera, R.; Shiraishi, Y. Novel microporous rhodium(II) carboxylate polymer complexes containing metalloporphyrin: Syntheses and catalytic performances in hydrogenation of olefins. *J. Catal.* **2005**, *232*, 186–198. [CrossRef]

30. Abello, L.; Bochu, B.; Gaskov, A.; Koudryavtseva, S.; Lucazeau, G.; Rumyantseva, M. Structural characterization of nanocrystalline SnO$_2$ by X-ray and Raman spectroscopy. *J. Solid State Chem.* **1998**, *135*, 78–85. [CrossRef]

31. Smith, E.; Dent, G. *Modern Raman Spectroscopy—A Practical Approach*; John Wiley & Sons Ltd.: Chichester, UK, 2005; p. 210.

32. Nakamoto, K. *Infrared and Raman Spectra of Inorganic and Coordination Compounds. Part. B: Applications in Coordination, Organometallic and Bioinorganic Chemistry*, 6th ed.; Wiley: Hoboken, NJ, USA, 2009; p. 406.

33. Silverstein, R.; Webster, F. *Spectrometric Identification of Organic Compound*; Wiley India Pvt. Ltd.: Delhi, India, 1997; p. 496.

34. Greiner, M.T.; Helander, M.G.; Tang, W.-M.; Wang, Z.-B.; Qiu, J.; Lu., Z.-H. Universal energy-level alignment of molecules on metal oxides. *Nat. Mater.* **2002**, *11*, 76–81. [CrossRef] [PubMed]

35. Lee, S.U.; Han, Y.-K. Density functional calculations on the ionization potentials of (CuPc)$_n$ (*n* = 1–6). *J. Mol. Struct. THEOCHEM* **2004**, *672*, 231–234. [CrossRef]

36. Minami, T.; Miyata, T.; Yamamoto, T. Work function of transparent conducting multicomponent oxide thin films prepared by magnetron sputtering. *Surf. Coat. Technol.* **1998**, *108*, 583–587. [CrossRef]

37. Liao, M.-S.; Scheiner, S. Electronic structure and bonding in metal porphyrins, metal = Fe, Co, Ni, Cu, Zn. *J. Chem. Phys.* **2002**, *117*, 205–219. [CrossRef]

38. Rumyantseva, M.N.; Gaskov, A.M.; Rosman, N.; Pagnier, T.; Morante, V. Raman surface vibration modes in nanocrystalline SnO$_2$: Correlation with gas sensor performances. *Chem. Mater.* **2005**, *17*, 893–901. [CrossRef]

39. Kovalenko, V.V.; Zhukova, A.A.; Rumyantseva, M.N.; Gaskov, A.M.; Yushchenko, V.V.; Ivanova, I.I.; Pagnier, T. Surface chemistry of nanocrystalline SnO_2: Effect of thermal treatment and additives. *Sens. Actuators B* **2007**, *126*, 52–55. [CrossRef]

40. Rumyantseva, M.N.; Gaskov, A.M. Chemical modification of nanocrystalline metal oxides: Effect of the real structure and surface chemistry on the sensor properties. *Russ. Chem. Bull.* **2008**, *57*, 1106–1125. [CrossRef]

41. Bordes-Richard, E. Multicomponent Oxides in Selective Oxidation of Alkanes Theoretical Acidity versus Selectivity. *Top. Catal.* **2008**, *50*, 82–89. [CrossRef]

42. Davydov, A. *Molecular Spectroscopy of Oxide Catalyst Surfaces*; John Wiley & Sons Ltd.: Chichester, UK, 2003; p. 641.

43. Flechter, K.; Kretschmann, A.; Steinrück, H.-P.; Gottfried, J.M. NO-Induced Reversible Switching of the Electronic Interaction between a Porphyrin-Coordinated Cobalt Ion and a Silver Surface. *J. Am. Chem. Soc.* **2007**, *129*, 12110–12111. [CrossRef] [PubMed]

44. Coe, B.J.; Glenwright, S.J. Trans-effects in octahedral transition metal complexes. *Coord. Chem. Rev.* **2000**, *203*, 5–80. [CrossRef]

45. Jones, T.E.; Rorabache, B.; Ochrymowycz, L.A. Simple models for blue copper proteins. Copper-thiaether complexes. *J. Am. Chem. Soc.* **1975**, *97*, 7485–7486. [CrossRef] [PubMed]

46. Amundsen, A.R.; Whelan, J.; Bosnich, B. Biological analogs. Nature of the binding sites of copper-containing proteins. *J. Am. Chem. Soc.* **1977**, *99*, 6730–6739. [CrossRef] [PubMed]

47. Wing-Wah Yam, V.; Man-Chung Wong, K. Luminescent metal complexes of d^6, d^8 and d^{10} transition metal centres. *Chem. Commun.* **2011**, *47*, 11579–11592.

48. Elhabiri, M.; Albrecht-Gary, A.-M. Supramolecular edifices and switches based on metals. *Coord. Chem. Rev.* **2008**, *252*, 1079–1092. [CrossRef]

49. Niwa, Y. X-ray photoelectron spectroscopy of reduced porphins. *J. Chem. Phys.* **1975**, *62*, 737–738. [CrossRef]

50. Case, D.A.; Karplus, M. X.alpha. multiple scattering calculations on copper porphine. *J. Am. Chem. Soc.* **1977**, *99*, 6182–6194. [CrossRef] [PubMed]

51. Tulyakova, E.V.; Fedorova, O.A.; Fedorov, Y.V.; Jonusauskas, G.; Anisimov, A.V. Spectroscopic study of mono- and bis(styryl) dyes of the pyridinium series containing azathiacrown ether residue. *J. Phys. Org. Chem.* **2008**, *21*, 372–380. [CrossRef]

52. Berdnikova, D.V.; Fedorov, Y.V.; Fedorova, O.A. Azadithiacrown ether based ditopic receptors capable of simultaneous multi-ionic recognition of Ag^+ and Hg^{2+}. *Dyes Pigment.* **2013**, *96*, 287–295. [CrossRef]

53. Garribba, E.; Micera, G.; Sanna, D.; Strinna-Erre, L. The Cu(II)-2,2′-bipyridine system revisited. *Inorg. Chim. Acta* **2000**, *299*, 253–261. [CrossRef]

54. Foley, J.; Tyagi, S.; Hathaway, B.J. The crystal structure and electronic properties of bis(2,2′-bipyridyl)-copper(II) bis(hexafluorophosphate). *J. Chem. Soc. Dalton Trans.* **1984**, *1*, 1–5. [CrossRef]

55. Pochtennyi, A.E.; Sagaidak, D.I.; Fedoruk, G.G. Composite sensor films phthalocyanine copper-polymer synthesized in plasma. *Vysokomolekulyarnye Soedineniya Ser. A Ser. B* **1997**, *39*, 1199–1205.

56. Trasatti, S. The absolute eletrode potential: An explanatory note. *Pure Appl. Chem.* **1986**, *58*, 955–966. [CrossRef]

57. Ponomarenko, S.A.; Rasulova, N.N.; Luponosov, Y.N.; Surin, N.M.; Buzin, M.I.; Leshchiner, I.; Peregudova, S.M.; Muzafarov, A.M. Bithiophenesilane-Based Dendronized Polymers: Facile Synthesis and Properties of Novel Highly Branched Organosilicon Macromolecular Structures. *Macromolecules* **2012**, *45*, 2014–2024. [CrossRef]

58. Chizhov, A.; Rumyantseva, M.; Vasiliev, R.; Filatova, V.; Drozdov, K.; Krylov, I.; Marchevsky, A.; Karakulina, O.; Abakumov, A.; Gaskov, A. Visible light activation of room temperature NO_2 gas sensors based on ZnO, SnO_2 and In_2O_3 sensitized with CdSe quantum dots. *Thin Solid Films* **2016**, *618*, 253–262. [CrossRef]